Journal of
Synchrotron
Radiation

ISSN 0909-0495

Received 20 June 2005
Accepted 23 October 2005

Silicon avalanche photodiodes for direct detection of X-rays

Alfred Q. R. Baron,[a]* Shunji Kishimoto,[b] John Morse[c] and Jean-Marie Rigal[c]

[a]SPring-8/JASRI, Hyogo, Japan, [b]KEK, Tsukuba, Ibaraki, Japan, and [c]ESRF, Grenoble, France.
E-mail: baron@spring8.or.jp

Silicon avalanche photodiodes (APDs) are discussed as fast X-ray detectors for synchrotron radiation. The emphasis is on 'direct' detection, where the X-ray is absorbed within the silicon APD itself, and, therefore, on use with medium-energy X-rays, <30 keV. The impact of APD structure on device performance is examined, and representative data from many different commercial devices are presented. Specific areas discussed include signal shapes, high-rate behavior, time resolution and pulse-height response. Data from several APD arrays are also presented, as is a detailed description of an integrated package system. Tables are included comparing commercially available devices, including arrays.

© 2006 International Union of Crystallography
Printed in Great Britain – all rights reserved

Keywords: APD; time-resolved measurements; fast counting; large dynamic range.

1. Introduction

This paper provides an introduction to the use of avalanche photodiodes, APDs, for direct X-ray detection. These devices, with single photon sensitivity and an intrinsically fast response, are the detector of choice in a variety of experiments. Of particular note is their extremely large dynamic range (the ratio of maximum count rate to noise rate is typically $>10^8$, and $\sim10^{10}$ is possible) and very good time resolution ($\sim$ns typical, <100 ps possible). Reasonable pulse-height resolution ($\sim$20%) is also relatively straightforward, even at high rates. Our main focus, and experience, is their use at synchrotron radiation facilities for medium-energy X-rays, <30 keV, but many results may be extrapolated to other work.

The outline of this paper is as follows. We review some of the basic properties of APDs including the silicon structure and the electronics, and some elementary concerns for high-rate experiments. Then we present data from several of the more useful single-element devices, and give a table of properties of many of the commercially available devices. We also discuss one well packaged system (integrated set of APD, amplifier, discriminator and counter) as an example of a general-use detector optimized for fast-counting experiments using synchrotron radiation. Finally we discuss array devices, presenting data from several different arrays, and a table comparing some commercial devices.

Development of APDs has been ongoing for the last 40 years or so (see Huth, 1968; McIntyre, 1966; Webb & Jones, 1974, and references therein). Much of the early work focused on noise issues and the use of APDs as a solid-state analogue to a photomultiplier tube: X-rays were mostly used as a probe of performance, and fast X-ray detection was not considered. After development of synchrotron radiation sources, pioneering use of APDs for fast X-ray detection was made by Kishimoto in the early 1990s (Kishimoto, 1991, 1992). Shortly thereafter, Baron and co-workers extended this to larger area and thicker devices that were more practical for synchrotron radiation detection (Baron & Ruby, 1993; Baron, 1994). In both cases it should be noted that much of the driving force for the work came from the field of nuclear resonant scattering, which requires fast detectors with good time resolution, and tends to be badly count-rate limited (see papers in Gerdau & de Waard, 2000). This field continues to place severe demands on detectors. Subsequently, the use of APDs as more general fast counters has been considered (Kishimoto, 1995; Baron *et al.*, 1997; Kishimoto *et al.*, 1998), and overviews can be found by Kishimoto (1998*a*,*b*) and Baron (2000).

Other notable points about APDs include their small size, typical for a solid-state device, and, as compared with photomultiplier tubes (PMTs), their relative immunity to magnetic fields. They also can be used in combination with scintillation crystals for higher-energy X-ray detection (Carrier & Lecomte, 1990; Moszynski *et al.*, 2003) including workers using them for positron emission tomography (PET). APDs can be used for very low energy X-rays, down to 50 eV, with due care regarding window structure (Gullikson *et al.*, 1995), and can also be operated at temperatures as low as 40 K (Yang *et al.*, 2003). Electron detection is also possible (Kishimoto, 2004) but electrons damage the surface and will eventually destroy the device.

2. APD basics

An APD is a diode doped so that when reverse bias is applied there is a region of high electric field ($\gtrsim10^5$ V cm^{-1}) which causes charge carriers entering that region to undergo gain due to impact ionization. APDs are typically operated in either a linear mode where the device has a well defined small-

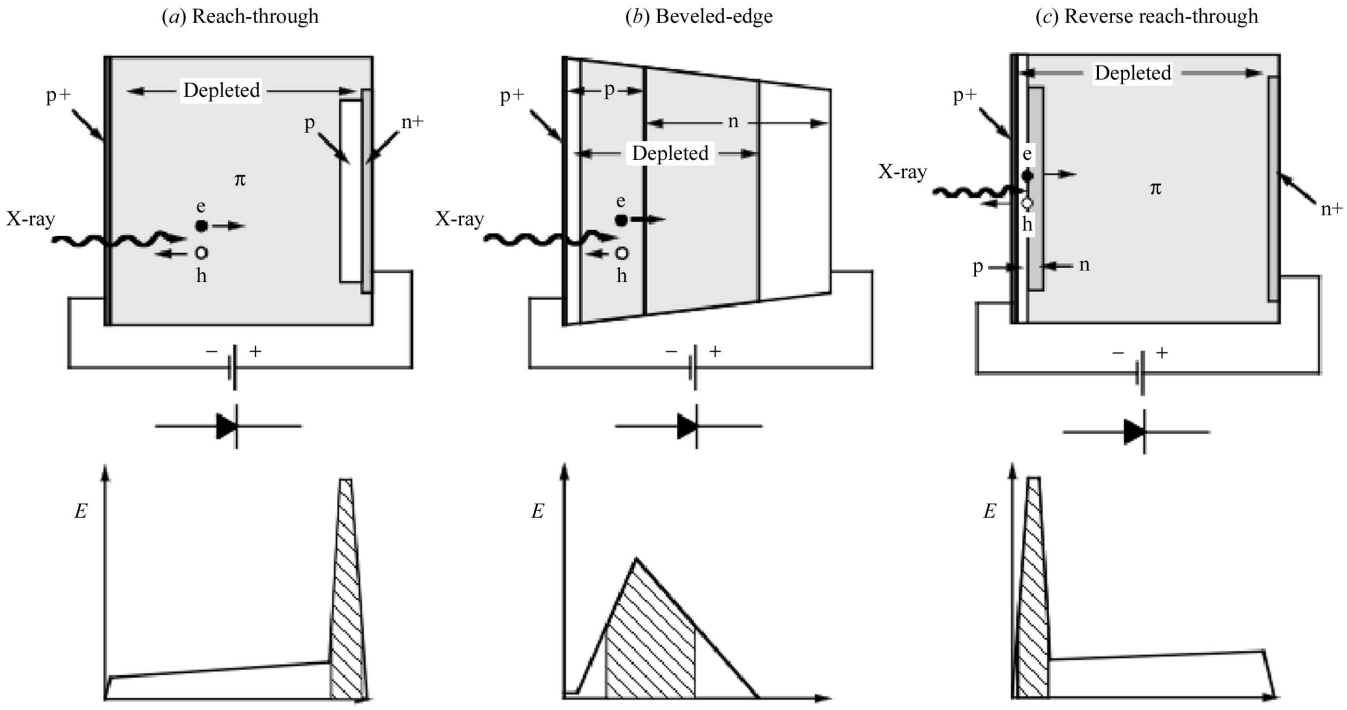

Figure 1
Schematic of the structure and field profile of several types of APDs. See text, §§2 and 5. The orientations are chosen so that, under bias, free electrons will move from left to right. Hatched sections of the field profile indicate the gain region. [After Webb *et al.* (1974) and McIntyre *et al.* (1996).] According to the usual diode convention, the left side is the anode and the right side is the cathode, with the X-rays shown entering through the anode. Reverse biasing (shown) is achieved by applying, say, positive HV to the cathode (right side) and holding the anode (left side) at ground.

signal gain (10 to 100 for most devices discussed here), or in a Geiger mode where they are biased above breakdown and a single electron leads to run-away gain. Here we discuss only linear operation, as Geiger operation leads to high noise rates and is generally most interesting for detection of very low energy (∼eV) photons.

Diagrams of several device structures are shown in Fig. 1. The depletion layer of the device consists of a low-field (drift) region and a high-field (gain) region. For modest-energy X-rays the dominant process in Si is photoelectric absorption, typically leading to a single electron having almost the energy of the incident X-ray. This electron then quickly loses energy to scattering processes in the silicon. On average, at room temperature, one electron hole–pair will be created for each 3.6 eV of energy deposited in the silicon. These electrons drift to the gain region of the device and are amplified. It is worth noting that at higher X-ray energies an increasing fraction of the X-rays will suffer Compton scattering (see Fig. 2), which, for most geometries, will cause the photon to go out of the detector without deposition of sufficient energy for detection. Thus, direct detection in silicon devices becomes increasingly inefficient at higher X-ray energies, owing both to decreased photoelectric absorption and to increased scattering out of the APD.

Two essential parameters for describing the response of an APD to X-rays are its active thickness and its capacitance. The active thickness of the device is that part of the silicon in which X-ray absorption will lead to subsequent electron amplification. This affects both the efficiency of the device and the time

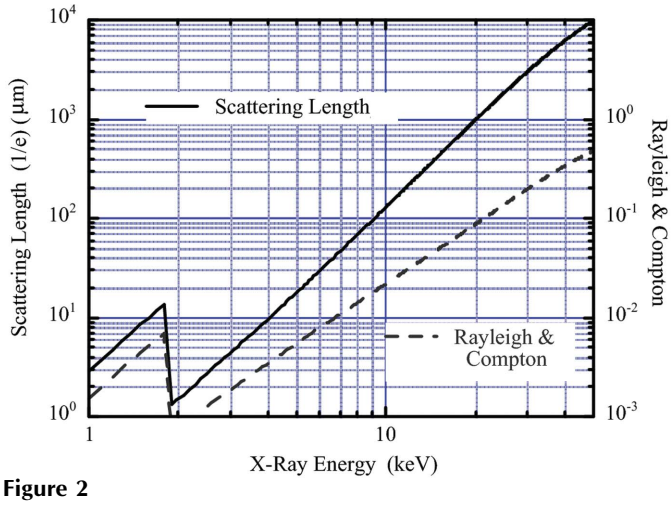

Figure 2
Absorption length in silicon as a function of X-ray energy. Note that the increasing importance of Compton and Rayleigh scattering at higher energies means that direct detection of X-rays in the device will become increasingly inefficient above 30 keV, even if the device could be made fairly thick. Calculations based on Cromer & Liberman (1981) and McMaster *et al.* (1969), using code based on Brennan & Cowan (1992).

resolution. The attenuation length in Si as a function of X-ray energy is shown in Fig. 2, allowing one to estimate the efficiency of APDs at different energies if the active thickness is known. Above 10 keV it is clear that an active thickness of 100 μm or more is desirable to have reasonable efficiency. Improvement can be gained by using devices at grazing incidence (Baron & Ruby, 1994) or stacking devices (Baron *et al.*,

1997), and one should note that the grazing incidence can be especially effective for small beam sizes. The high-field drift velocity in Si is about 100 μm ns^{-1} (Jacoboni *et al.*, 1977). Since X-rays tend to penetrate and (to a first approximation) uniformly illuminate the active thickness of Si, the time resolution is generally not better than the active thickness over the drift velocity (assuming, of course, normal entry into the device). This means that there is typically a trade-off between device efficiency and time resolution: for example, an APD with a 100 μm active thickness will generally not have better than about 1 ns time resolution, while to get below 100 ps time resolution the active thickness should be ∼10 μm or less.

The APD capacitance, determined by the area and the thickness of the depletion region, affects both the height and the width of the voltage pulse from the device. In detail, considering the APD as a parallel-plate device with constant field (see Knoll, 2000), one finds that the rise time of the voltage signal will be governed by the details of the charge transport within the device, while the fall time is not shorter than the RC time constant of the diode capacitance and the amplifier input impedance (*e.g.* RC = 1 ns for a 20 pF diode capacitance into 50 Ω). Meanwhile, the voltage signal height scales inversely with the device capacitance, for a fixed gain, so devices with lower capacitance (smaller areas, thicker depletion regions) generally provide larger and faster signals.[1]

Detailed discussion of device structure, especially as related to noise properties of the APD, can be found by McIntyre (1972) and Webb *et al.* (1974), while reviews of charge transport in silicon can be found by Sze (1981) and Jacoboni *et al.* (1977). Here we note that an important parameter in device performance is the ratio of electron gain to hole gain on passing through a region of the device: statistical fluctuation in gain (noise) is reduced when one carrier type undergoes much stronger multiplication than the other. In silicon, electron multiplication dominates strongly over hole multiplication, so that noise properties are relatively good. This is in contrast with other materials (Ge, InGaAs and derivatives) where the coefficients are more nearly equal. However, some recent work suggests that if very narrow gain regions are used the amplification properties are improved, even for cases when the gain is similar for electrons and holes (Rees & David, 2003), so that one might hope for more progress with non-silicon APD structures in the near future.

3. Electronics

For most of the applications discussed here, the APD is followed by a wide-bandwidth (∼GHz) voltage amplifier. While other types of amplifiers have been considered, the voltage amplifier seems to be a reasonable compromise between speed and convenience on the one hand, and noise characteristics on the other. In cases where it might be useful to sacrifice speed for better noise performance (*i.e.* to get to very low X-ray energies with a larger area device), one might reconsider a transimpedance amplification scheme. Going the opposite direction, toward higher bandwidths, might also be considered but one should note that the minimum X-ray pulse separation at most synchrotron radiation facilities is 2 or 3 ns. Voltage amplifiers are available in pre-packaged form from several manufacturers, but also can be home or custom built. The main advantage of the latter is the ability to tailor the amplifier to the detector package design, and to place it very close to the APD, reducing noise and reflections [see Baron *et al.* (1997) for a simple useful low-power design]. Practically speaking, the relatively high bandwidth of most APD set-ups requires due care in design of both the APD enclosure and the interface with electronics, to avoid possible reflections, noise and amplifier oscillation. Scope traces from various APD structures discussed in §5 are shown in Fig. 3.

Downstream electronics usually include both a discriminator and a counter. There are no special requirements for these beyond the more obvious ones: appropriate input impedance (typically 50 Ω), a discriminator threshold range appropriate to the signal height out of the amplifier, and low dead times for higher-count-rate experiments. Generally, in this time region, NIM or ECL level logic signals are standard. Discriminators can be bought from Phillips Scientific (http://www.phillipsscientific.com/) and Ortec (http://www.ortec-online.com/) among others, while counters are available from many companies. It can be somewhat difficult to find devices operating with less than 5 ns dead-times or pulse widths; however, one company that makes faster (300 MHz) discriminators and counters (for CAMAC) is Technoland (http://www.tcnland.co.jp/). It is worth noting that with the very fast rise-time signals often used in the fastest (sub-ns) timing experiments, and with the relatively good intrinsic pulse-height resolution of the devices, there appear to be no strong improvements to the time resolution by using a commercially available constant fraction timing system (such as the 935 CFD from Ortec). Most of the work discussed here has been performed with leading-edge discriminators.

4. High rates

One of the main interests in APDs stems from their ability to count at rather high rates: ns pulse widths hint at maximum count rates of several hundred Mcounts s^{-1}. In practice, however, high rates require some care, especially as a detector known to be 'fast' can sometimes lead the user to push things a bit. If even modest rates are of interest, then it is very important to have some idea of the counting *system* dead-time, to properly judge pile-up effects. Typically, for an APD with the wide-bandwidth electronics discussed here, the *detector* dead-time is indeed of the order of ns, with a worst case of about 10 to 20 ns for very large capacitance devices. However, the *system* dead-time includes contributions from the dead-time of the discriminator and the counter. In addition, and especially notable at a synchrotron radiation facility, the

[1] This is a useful rule of thumb, best applied for comparing devices with the same structure and different areas. If comparing devices of different structures, some care is needed as structural changes imply changes in field profiles and carrier transport properties that may affect signal heights and rise times.

source time structure is very important: the electron bunch structure in the storage ring, which directly gives the time structure of the incident X-ray pulses, can vary widely. For example, at SPring-8 the minimum bunch spacing is 2 ns, but a substantial part of operating time includes spacings of 24 to 200 ns, which can easily be the limiting system dead-time.

A general discussion of high-rate behavior can become rather involved, but a first approximation is both relatively easy and useful. Assuming that the system dead-time, τ, is known and well defined, and a lower level discriminator only is being used, then a simple non-paralyzable model (see Knoll, 2000, pp. 119–122) allows one to write the true rate, n, from an ideal linear system without dead-time in terms of the measured rate, m, as

$$n = m/(1 - m\tau). \quad (1)$$

Generally, this is a reasonable approximation at lower rates and, in fact, other models (*e.g.* the paralyzable model) give the same result to first order in $n\tau$. It also gives the correct high-rate limit if the bunch spacing in the storage ring is the limiting dead-time, and all bunches are uniformly filled. Note that in the event that an upper-level discriminator is used to make a window around the single-photon pulse height, this form is wrong [see also the discussion by Bateman (2000)].

Several checks of APD behavior at high rates have been carried out using different devices and electronics and with different levels of sophistication (Kishimoto, 1995, 1997; Baron *et al.*, 1997). Examples are shown in Fig. 4. Dead-times of ~3 ns have been achieved in favorable operational modes with relatively fast, 300 MHz, discriminators and counters, with maximum measured count rates of $\sim 10^8$ (Kishimoto, 1995). The maximum achievable rate can also be increased by using a stack of devices in a transmission geometry (Kishimoto *et al.*, 1998), which is sometimes referred to as a 'telescope'. Stacking devices, however, are complicated by the fact that absorption in upstream devices leads to non-uniform count rates in the stacked detectors, with the front detector at higher rates. There can also be a sensitive dependence on the X-ray energy as the absorption changes. An alternative is an array of devices at grazing incidence (see §8) to avoid the absorption-induced non-uniformity. However, this introduces sensitivity to the spatial distribution of the detected beam. Finally, for the

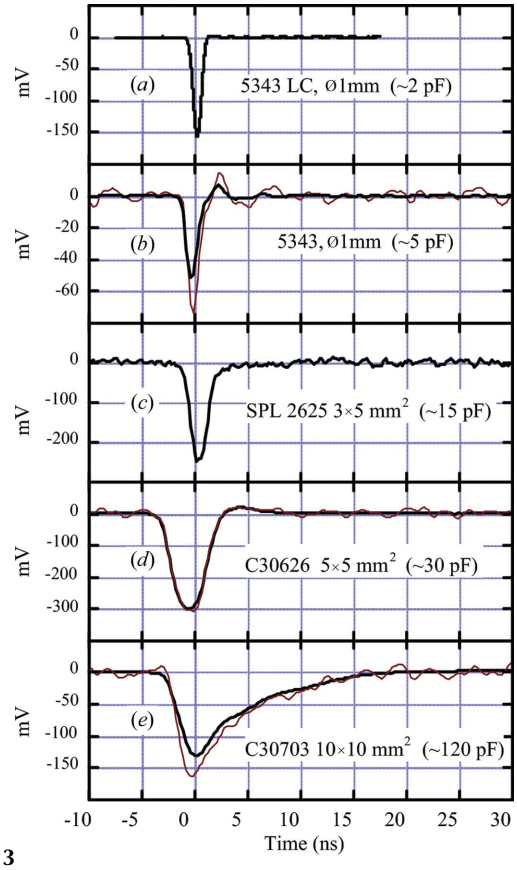

Figure 3
Scope traces from several different APDs (see text, §5 for details) using the amplifier discussed by Baron *et al.* (1997) (*a*, *b*, *d*, *e*) and a Keycom LNA-012 (*c*). The heavy solid line shows the response averaged over many events, while the thin line shows a single event with noise [average only in (*a*) and single event only in (*c*)]. Note that the exact pulse heights relative to noise will depend on the APD gain, and the signal shape can also be affected by parasitic capacitances that are not included in the estimates shown. The overshoots visible on the average signal (*b*) and (*d*) result from less than ideal coupling to the amplifier. Also note that for the slower signals in (*d*) and (*e*) a smaller bandwidth amplifier, as used in the package system discussed in §7, is more appropriate and should be less noisy.

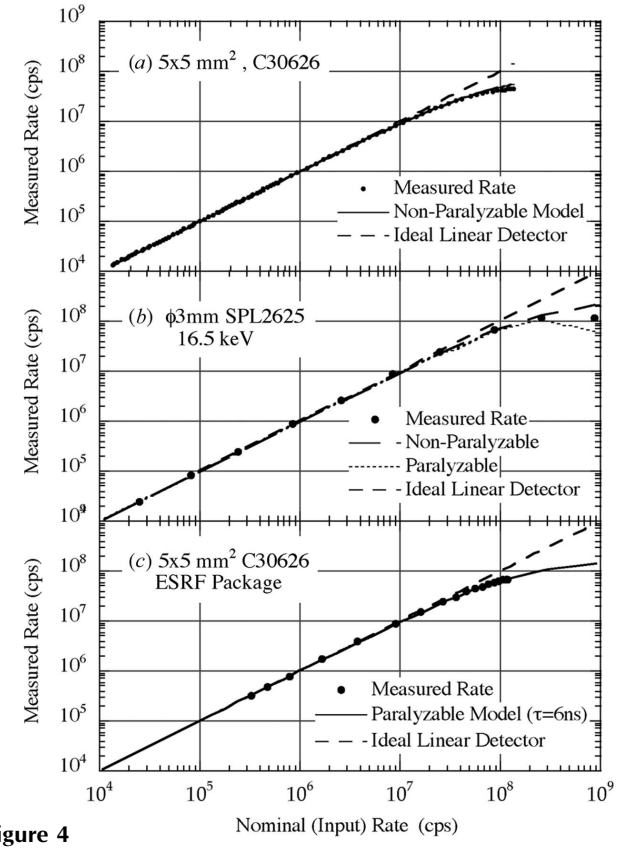

Figure 4
High-count-rate behavior of single-element devices in different configurations. (*a*) 5 mm × 5 mm APD (C30626) followed by a Phillips 708 discriminator and an ESRF counter card, with an asymmetric storing-ring filling pattern. Dead-time contributions include the discriminator pulse-pair resolution (~7 ns), the counter dead-time (~5 ns) and the 2/3 filling mode of storage-ring operation. (*b*) Single-element SPL2625 device using Technoland discriminators and counters. (*c*) ESRF package system with baseline restoration in a near-uniform fill mode.

Table 1
Properties of some single-element APDs.

Company	Model	Size	Operating voltage	Active thickness (μm)	Capacitance (pF mm^{-2})†	Gain†	Time resolution FWHM/tail (ns)
Perkin-Elmer (PKI/EG&G)	C30626	5 mm × 5 mm and smaller	300–400	∼110	1.2	50–150	∼1/3
	C30703	10 mm × 10 mm	350–450	∼110	1.2	50–150	∼1/4
	Prototype‡	10 mm × 10 mm	350–450	∼180	<1	50–150	1.7/7
	C30719‡ reverse	5 mm × 5 mm	350–450	<10	–	∼50	0.17/2–3§
Hamamatsu	SPL2625‡	Diameter 3 mm, 3 mm × 5 mm	500–700	∼130	∼1	30–50	1.3/3
	S238X	Diameter 0.2–5 mm	∼150	∼30	6	50–100	0.3/5§
	S534X	Diameter 1 mm, 3 mm	∼150	∼ 10	16	∼50	∼0.08/<2
	S534X LC‡	Diameter 1, 3, 5 mm	∼250	∼20	5	∼50	∼0.15/<2
	S8644-XXK reverse	Diameter 0.2 to 5 mm, 5 mm × 5 mm	∼400	∼7	3	∼50	Not tested
Advanced Photonix Inc.	LAAPD beveled-edge	Diameter 3–16 mm	∼2000	30–50	∼1	∼200	∼0.4/>5§
Radiation Monitoring Devices	S0814	8 mm × 8 mm	∼1700	30–50	∼1?	300–2000	∼0.4/>10§
	S1315 beveled-edge	13 mm × 13 mm					

† Capacitance and gain values are from the literature. ‡ Device not in catalogue – inquire directly of the company. § The tail of the time response may be reduced by higher discriminator threshold setting.

case where the source bunch spacing (synchrotron operational mode) is the main source of dead-time, some increase in maximum count rate for a single device may be gained by fanning out the signal and using several discriminator levels corresponding to 1, 2, 3,... photon events (Toellner *et al.*, 1994).

We emphasize two points before leaving the subject of high-rate experiments. The first is that while a fast detector easily adds to the convenience of an experiment, to use it effectively requires some care. Applying the above model, taking $m\tau \simeq 0.1$, or a measured rate of 20 Mcounts s^{-1} for a 5 ns dead-time, an uncorrected measurement will have a 10% error (integral non-linearity) and one expects that the corrected rate is good at the level of 1%, assuming the proper dead-time is known. At $m\tau = 0.01$, a 2 Mcounts s^{-1} rate for a 5 ns dead-time, uncorrected rates should be accurate at the 1% level and corrected rates at the 0.01% level. It is clearly important to take this into account to make accurate measurements. The second point, evident in Fig. 4, is that at higher count rates ($n\tau > 0.3$) simple models, and even more complicated ones, tend to fail. In fact, issues such as the AC coupling the amplifier, and voltage droop owing to increased current in the APD and a limiting resistor, can change the effective detector characteristics at high rates. Thus extreme care is needed in the higher rate regime and, probably, a calibration measurement is necessary, in a configuration almost identical to the experimental one.

5. Devices and time resolution

APDs are commercially available from several companies. Here we mention devices from Perkin-Elmer Instruments (PKI) (formerly EG&G) (based in Quebec, Canada; http://optoelectronics.perkinelmer.com/),[2] Hamamatsu Photonics (based in Hamamatsu, Japan; http://www.hamamatsu.com/), Advanced Photonics Inc. (API) (based in Camarillo, CA, USA; http://www.advancedphotonix.com/) and Radiation Monitoring Devices (RMD) (based in Watertown, MA, USA; http://www.rmdinc.com/). PKI and Hamamatsu specialize in reach-through devices, while API and RMD focus on beveled-edge devices. In general, each type of device has different properties, and even different models within a class can vary significantly. Table 1 summarizes the properties of many devices with some details discussed below.

Reach-through devices, with structure similar to Fig. 1(*a*), have a long history (see, for example, Webb & Jones, 1974). At present, devices of similar structure and behavior can be bought from both PKI and Hamamatsu, with larger single-element devices available from PKI (10 mm × 10 mm and 5 mm × 5 mm) and smaller devices from Hamamatsu (3 mm × 5 mm and 3 mm-diameter sizes are typical). Smaller devices are also available from PKI, but are not readily supplied in packages without windows, while Hamamatsu also make several array structures based on the 3 mm × 5 mm device (see §8). These devices tend to have larger active thicknesses, 100 to 180 μm, and time resolutions of 1 to 2 ns full width at half-maximum (FWHM). In terms of X-ray detection, their main notable property is that they have comfortably large areas and a single device is reasonably efficient at normal incidence. As such, for example, they are used in the general purpose packages mentioned in §7. Devices from both companies can be purchased without a back, or in a transparent form, so that stacking is possible to increase dynamic range and/or efficiency at higher energies (Hauger *et al.*, 1994; Baron *et al.*, 1997; Kishimoto *et al.*, 1998; Shvyd'ko, 1999).

A variety of epitaxial reach-through structures are also sold by Hamamatsu, including the S238*X* and S534*X* series (*X* to be replaced by a number correlating with device diameter). The former was the first device used for fast X-ray detection (Kishimoto, 1991, 1992) while the latter was shown to have ∼100 ps time resolution (Kishimoto, 1994), made possible by

[2] Note that original work on some of these devices was carried out by RCA, then moving to EG&G Optoelectronics. After EG&G bought out Perkin-Elmer, EG&G changed its name to PKI.

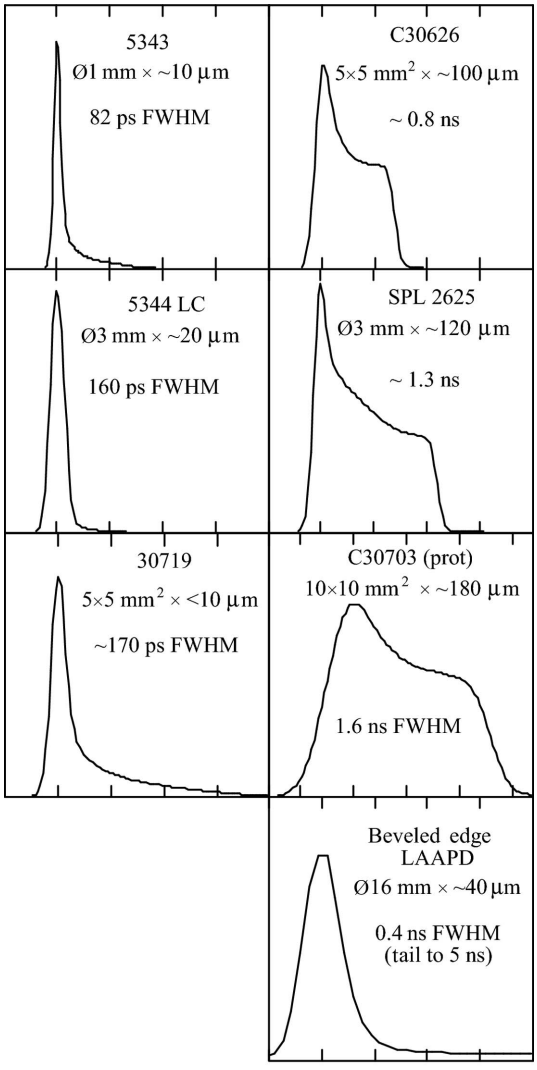

Figure 5
Time response of several different types of APDs, as listed. Full horizontal scale is 2.5 ns in each case. See §5 of the text for discussion.

its rather small, ~10 μm, active thickness. Fig. 5 shows the time response of the S5343 device, with a measured 82 ps FWHM, suggesting a time resolution of ~72 ps if the source pulse width is subtracted. The very short tail on the time response (<2 ns at 10^{-5} of the maximum) is also useful in some cases, especially for nuclear resonant scattering. However, a difficulty with these devices is that their thin depletion region leads to relatively large capacitances (see Table 1) so the pulse height is small. For example, attempts to match the <100 ps time resolution of the S53543, a 1 mm-diameter device, using a 3 mm-diameter S5344 device having nominally the same structure failed because the signal height decreased so much that amplifier noise blurred the resolution to ~140 ps. Thus the development of a low-capacitance version of this series, S534X LC, where the depletion region was increased was greeted with enthusiasm. For the LC device the active thickness was also increased, to ~20 μm, which increased the overall time resolution to ~150 ps FWHM (see Fig. 5). However, the signal-to-noise ratio was dramatically improved, and the tail of the time response behaved similarly to the original device. This device, then, is especially interesting as a fast low-energy X-ray detector (low energy because it is thin) and for cases where a short time response is essential.

The third structure shown in Fig. 1, the 'reverse'-type reach-through device, is a new design, with devices made both by PKI (McIntyre *et al.*, 1996; Lecomte *et al.*, 1999) and Hamamatsu (Dieters *et al.*, 2000; Renker, 2002). This structure was developed in response to the need of the high-energy physics community for $>10^5$ devices for the CMS calorimeter at CERN (Dieters *et al.*, 2000). Here, as compared with the earlier reach-through design, the gain region is moved up to the front so that the active thickness is drastically reduced, while the depletion layer thickness is kept large. This makes the device, designed for use with scintillators, deliberately less sensitive to penetrating particles, while preserving a relatively low capacitance. As regards X-ray detection, these devices are most interesting at low energies when the loss owing to the limited active thickness is not so severe. In this sense they are similar to the S534X LC series. They are also potentially interesting when good time resolution is needed. For the case of the larger area (5 mm × 5 mm) C30719 device tested in Fig. 5, the time resolution could easily have been degraded by electrical noise, as discussed above. One also can expect there to be large event-to-event gain fluctuations in the reverse structure since a large fraction of the X-rays will be absorbed within the gain region and be only partially amplified. It might be interesting then to consider a fast constant fraction discriminator to improve the timing performance of the reverse structure devices.

The 'beveled-edge' device (Fig. 1*b*) dates back to work in the 1960s at General Electric (see Huth, 1968, and references therein) and, interestingly, the essential idea discussed here, using an APD followed by a discriminator and counter, was discussed very early on (Locker & Huth, 1966), in contrast to the focus on noise properties that seems to have dominated the discussion of reach-through devices. At present, beveled-edge devices are available from API and RMD, and discussion of some of the details of these devices can be found by Moszynski *et al.* (2000) for API devices and Squillante *et al.* (1985) and Farrell *et al.* (2000) for RMD devices. Particular advantages of the beveled-edge structure are the possibility to go to very large areas (*e.g.* a 200 mm^2 device is available from API) and very high gains, especially in devices from RMD (Farrell *et al.*, 1994). Also, the distributed nature of the gain region in these devices facilitates their operation at low temperatures, down to 40 K (Yang *et al.*, 2003). However, the presence of a low-field region at the front of the device leads to a tail in the time response (Baron & Ruby, 1993), as seen in Fig. 5. In addition, this region, and the rather wide gain region, can lead to a pulse-height response with a long tail, or even multiple peaks at high gains. These factors, along with a certain lack of device stability, including device failure, in devices tested some years ago, have led us to favor reach-through devices for X-ray detection. We note the recent development of a grooved planar device (without the bevel)

by RMD (Farrell *et al.*, 2000; Shah *et al.*, 2001), but they have not been investigated, to our knowledge, as regards their time response. Their pulse-height response, however, is very similar to that of the beveled devices, and one might expect the time response to be as well.

Before leaving the subject of time response of the devices, it is worth emphasizing two caveats. The first is that the time resolution (FWHM) of the faster devices is noise sensitive (see also the discussion by Hauger *et al.*, 1994). An extreme case was mentioned above where a larger-area version of the S534X series had significantly poorer time resolution than a smaller-area version (~80 ps for the 1 mm-diameter 5343 *versus* ~140 ps for the 3 mm-diameter 5344), but this is also true for other devices. Generally, the lower the capacitance, the larger the signal height and the smaller the effect of noise. However, even with the S534X LC ('low capacitance') models, the time resolution seems to vary from 140 ps for a small-area model to 160 ps for a larger-area model. The other point worth mentioning is that not all devices of a given type are the same. On the one hand there can be deliberate changes introduced by the manufacturer and, on the other, there is often device-to-device variation within a class, depending on date of manufacture *etc.* This applies to operating voltages, gains and even to field distributions within the device.

6. Pulse-height response

It is sometimes desirable to make use of the pulse-height response of the APD for energy discrimination. This can be done with the fast signal by just using a lower-level discriminator or, in some cases, by setting both a lower level and upper level threshold.[3] It can also be done using slower (~μs) nuclear electronics, with good results [10% typical resolution, even 5% possible for cooled devices at low gains (Kishimoto, 1998*a*,*b*]; however, the slower electronics partially defeat the purpose of a fast detector. Thus we focus on discrimination of the fast signals from the ~GHz bandwidth voltage amplifiers discussed above. Experimentally this has been investigated with the thicker types of reach-through devices from PKI (Baron *et al.*, 1997) and Hamamatsu (Kishimoto *et al.*, 1998). Fig. 6 shows measured responses for a 5 mm × 5 mm C30626 device from PKI and a 3 mm-diameter SPL2625 device from Hamamatsu. At lower X-ray energies, 5.9 keV, a relatively clean spectrum of about 20% FWHM is observed, while at higher-energy X-rays a tail develops as the X-rays penetrate into the gain region. Thus, one can expect that the pulse-height distribution will depend sensitively on the type of device as well as the incident X-ray energy.

The high-rate behavior of the pulse-height distribution is also shown, and in general it is fine up to rates of 10 Mcounts s^{-1} or so, and is even not bad at 47 Mcounts s^{-1} from the smaller device (Fig. 6*c*). It is worth noting that there is a shift in centroid of the response to low energies (voltages) as the rate is increased. This results from the AC coupling of the amplifier system: the net charge through the system must be zero, so that a fast negative going signal is accompanied by a slow positive overshoot of equal area, the timescale of which is set by the low-frequency cut-off of the system. At high rates the positive overshoot builds up and leads to a decrease in the signal height relative to a fixed external discriminator threshold. The effect of the shift will generally scale with APD capacitance: devices having smaller capacitances generally have shorter output pulses, so while the baseline shift will have the same integral as the signal pulse, it will be a smaller fraction of the signal height than for a larger capacitance

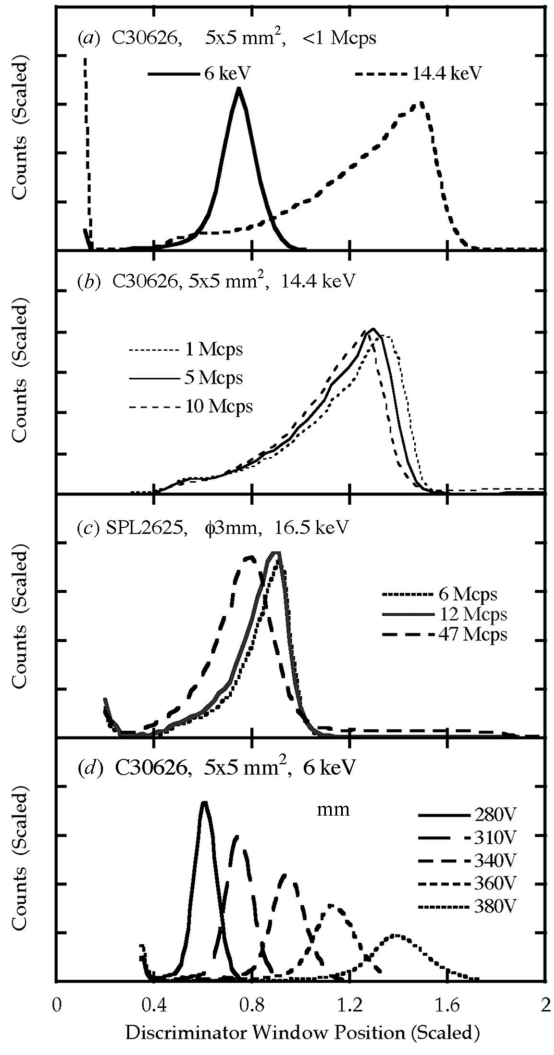

Figure 6
Pulse-height response of reach-through APDs with fast electronics as measured by scanning the window of a fast discriminator. (*a*) 6 and 14.4 keV response of the 5 mm × 5 mm C30626 device from PKI at low rates. Note the tail in the 14.4 keV response owing to penetration into the gain region (see Baron *et al.*, 1997). (*b*) Effect of count rate at 14 keV. (*c*) Pulse-height response with a 3 mm-diameter SPL2625 from Hamamatsu at 16.5 keV (see Kishimoto, 1998*b*). Note the centroid shift as the rate increases in (*b*) and (*c*). (*d*) Response of the C30626 device (in the ESRF package system, see §7) as a function of operating voltage for 6 keV X-rays at about 1 Mcount s^{-1}. The broadening from 21% (280 V) to 27% (380 V) with increased gain is typical for this device. Vertical and horizontal scales have been adjusted for convenient display; however, the zero is well defined.

[3] The Phillips Scientific model 730 discriminator has both upper and lower levels.

device (see also the discussion in §7 where additional electronics are used to reduce the baseline shift in the ESRF package system).

7. Package systems

A package system, including the APD and most, or all, of the downstream electronics, is extremely convenient for users, or beamline scientists, who do not wish to become involved in the details of the detector design and operation. Thus some synchrotron radiation facilities, including the NSLS at Brookhaven and the ESRF in Grenoble, have made such systems. Here we discuss the ESRF package in some detail. The NSLS package (Kuczewski & Siddons, 2002) is similar, providing the detector head with APD and amplifier, and then a NIM module with power supplies and discriminator. The NSLS package is designed with the 53 MHz bunch frequency of NSLS in mind, and does not have a baseline restoration circuit.

The ESRF package consists of a miniature APD head, and a NIM format 'ACE' configurable electronic controller unit (see Fig. 7*a*), with supporting software for both *SPEC* and *LabVIEW*. A GPIB interface is used. Notable hardware features include:

(i) A very small APD head (see Fig. 7*b*) that is easily exchanged to allow use of different devices or different mounting geometries (side or front window) to match experimental needs.

(ii) A low-noise 500 MHz bandwidth pre-amplifier that allows operation at energies down to 3 keV with a PKI C30626 device and less than 0.1 counts s^{-1} dark rate.

(iii) Active and passive current limiting to protect the APD, as well as a high voltage (HV) shutdown option on sustained overload, as might arise if the APD were placed in the direct beam.

(iv) A temperature monitor that is interfaced with the HV control to allow the bias to be adjusted to compensate for temperature-induced gain variations. In practice, with a temperature coefficient of about 1.3% K^{-1} for a typical PKI 36206 APD at a gain of 100 and the low power-consumption of the pre-amplifier, <300 mW, this has not been needed. Note that varying the APD bias to stabilize the gain is considerably easier than maintaining the APD at a constant temperature.

(v) A 100 MHz counter/single-channel analyzer that can operate at burst rates up to 180 MHz.

(vi) Upper and lower discriminator thresholds configurable to allow integral or window counting modes.

(vii) Feedback of the operating HV to stabilize device gain at high rates where the larger current in the protection resistor leads to droop in the voltage across the APD.

Notable control features include: (i) a touch-screen graphical display for convenient local set-up; (ii) a multi-channel histogram option (by scanning a discriminator window) and the possibility to use this to automatically set the lower-level discriminator threshold; (iii) the possibility to synchronize multiple count-times with external triggers with better than 10 ns precision.

The combination of these features creates a flexible and robust system that is now in widespread and routine use at the ESRF. The general behavior has been partially covered in previous sections, including count rates up to 50 Mcounts s^{-1} with 60% efficiency (see Fig. 4) and ~20% pulse-height resolution (Fig. 6).

Two notable features were included to improve the high-rate behavior of the system. A base-line restoration circuit (a double Schottky diode design) was included in the ACE module to help remove the affects of the AC coupling discussed in §6. Simulations using a pulser (see Fig. 8) showed that this leads to a significant reduction in the effect on the peak heights so that, despite the relatively high capacitance (~30 pF) of a 5 mm × 5 mm C30626 device, rates up to 50 Mcounts s^{-1} were possible. In addition, a fixed discriminator reset time is included and is set at slightly longer (5.4 ns) than the pulse width from a single photon so that the dead-time should not be affected by X-ray energy. This, in

(*a*)

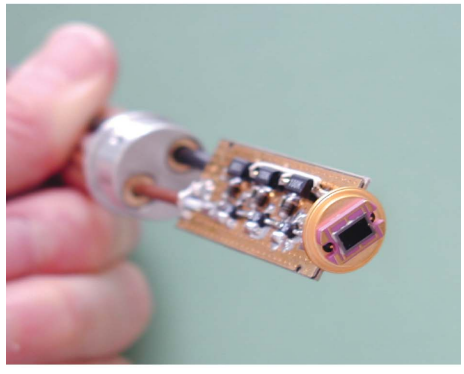

(*b*)

Figure 7
The ESRF package system. (*a*) The 'ACE' NIM format controller module and an assembled APD detector head package. Note the front panel NIM/TTL inputs that permit external hardware synchronization. (*b*) The open APD head, fitted here with a 3 mm × 5 mm SPL2625 device from Hamamatsu. The layout of the three-stage preamplifier can be seen.

Table 2
APD array devices. 'Type' refers to the assembly: M = monolithic, A = assembled from separate devices, R = replaceable elements.

Company	Device structure	Type	Array pixels	Pixel size	Dead-space (mm)	Reference
Perkin-Elmer (PKI/EG&G)	C30985†	M	1 × 25	∼0.4 mm × 0.3 mm pitch	∼0.05	Webb & McIntyre (1984)
	†	M	1 × 32	0.35 mm × 0.15 mm pitch	∼0.05	Trakalo *et al.* (1987)
	†	M	1 × 128	2 mm × 0.15 mm pitch	∼0.05	Webb & Dion (1991)
Hamamatsu	S238X	M	1 × 16	Diameter 1 mm or 1 mm × 1 mm	0.1	Hara *et al.* (1996)
	‡	M	1 × 32	3.8 mm × 0.5 mm	Variable	Nonaka *et al.* (1996)
	S534X LC	M	1 × 16	2.5 mm × 1 mm	0.1	Baron *et al.* (2001)
	SPL2625	A	2 × 16 and 2 × 4	3 mm × 5 mm	1	Kishimoto *et al.* (2003)
	50 µm§	M	2 × 4	1 mm × 0.5 mm	0.1	Kishimoto *et al.* (2003)
	S5343 LC	AR	1 × 10	Diameter 3 mm	1	This work
Advanced Photonix Inc.	Beveled-edge	M	8 × 8	1.3 mm × 1.3 mm	0	Gramsch *et al.* (1993)
	Grooved			0.5 mm × 0.5 mm	0	Gramsch *et al.* (1994)
Radiation Monitoring Devices	Planar beveled	M	4 × 4	2.1 mm × 2.1 mm	0.4	Farrell *et al.* (2000)
	Grooved		8 × 8	13 mm × 13 mm	0.4	
	Planar beveled grooved	M	14 × 14	2 mm × 2 mm pitch	0.1	Shah *et al.* (2001)
	Planar beveled Anger¶	M	1¶	14 mm × 14 mm¶	0¶	Levin *et al.* (2004)

† While these have variable structures in the plane of the device, their structure normal to the surface is basically the same reach-through device discussed in the text (*e.g.* the C30703 structure). ‡ Several devices were constructed of varying structures for test purposes. § This is a specially developed 50 µm reach-through device on a 50 µm-thick wafer. ¶ This device uses leads in each corner to measure relative signal heights and so determine the event position, similar to an Anger camera.

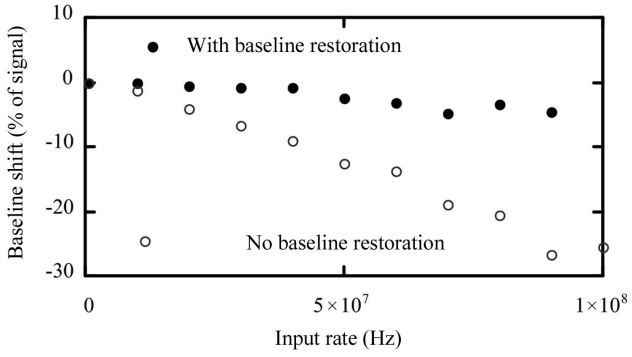

Figure 8
Effect of the baseline restoration circuit in the ESRF package. Reduction in effective pulse height as a function of input pulse rate both with and without the restoration circuit. This test was carried out using a frequency generator adjusted to simulate the APD signal pulse shape.

principle, allows a dead-time correction to be determined for a given storage-ring fill pattern that is independent of X-ray energy.

8. Arrays

Array devices, either one-dimensional or two-dimensional, are interesting for covering large areas to obtain position-resolved information and, in some cases, to allow higher count rates or to make a more efficient detector. For example, APD arrays are either in use, or could be immediately useful, in nuclear resonant scattering experiments or fast intensity correlation measurements. Arrays can be either monolithic, with multiple elements on a single piece of silicon, or assembled, with separate silicon pieces placed close together. Assembled arrays offer the advantage that devices can be selected according to their performance, and, in some cases, can even be replaced if they die; however, they also generally have larger dead-space between elements. Table 2 lists a variety of array devices, and we discuss some in more detail below.

PKI has produced several linear arrays based on their standard reach-through structure (∼110 µm active thickness) with specialized guard-rings and electrodes (see Table 2). These are notable for their small element size, developed with an eye toward fiber-optic applications, and for the use of bump-bonding on the back (cathode) to make electrical contact to each element. Brief tests of one of the 25 element linear arrays (C30985), see Fig. 9, showed timing performance similar to the parent C30703 structure, while element sizes were ∼275 µm (FWHM) along the array direction and ∼440 µm (FWHM) perpendicular to the array direction, with flat top regions of ∼150 µm × 220 µm. The dead-space, FWHM to FWHM, is about 50 µm. It is worth noting that the bump-bonding has the advantage that there are no bond wires to shadow the front surface. It also inverts the signal polarity relative to the more typical case of taking the signal from the front surface (anode), so both the amplifier and, possibly, the high-voltage bias system require modification (inversion) if taken from a typical set-up for a single-element device.

Hamamatsu makes assembled arrays of their thicker (SPL2625) structures (∼140 µm active thickness), with typical element sizes of 3 mm × 5 mm, and thus rather different than the small-element monolithic devices made by PKI. These large-element assembled arrays (see Fig. 10) are useful for covering larger areas, especially for nuclear inelastic scattering experiments, and, possibly, for synchrotron-radiation-based perturbed angular correlation measurements. Comparing these to the PKI 10 mm × 10 mm devices, one notes that there are losses owing to the 1 mm dead-space, and increased complexity because several channels of electronics are needed. However, this is offset by the large total area of the array and, in some cases, by the improved signal to noise arising from the smaller capacitance (smaller area) of a single element, making it easier to detect lower-energy X-rays. We

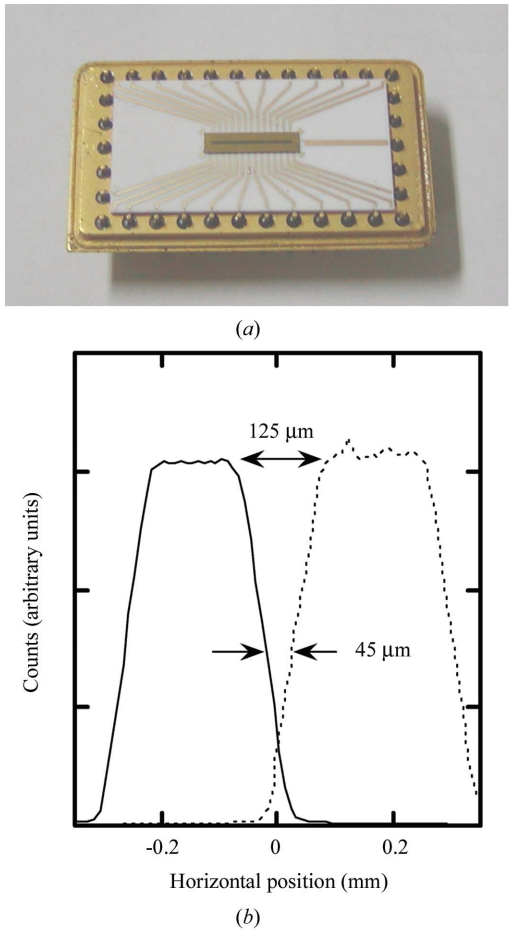

Figure 9
25 element array from PKI (C30985). The photograph in (*a*) shows one device. The central piece of silicon is 2 mm × 9 mm. In (*b*) the counts from two adjacent elements are measured when the array is scanned through a small X-ray beam. The elements are ∼250 to 300 μm (FWHM), with flat tops of ∼150 μm. The dead-spaces are indicated. Note that a scan in the orthogonal direction (not shown) gives the element width to be ∼440 μm (FWHM) with a flat top of about 220 μm.

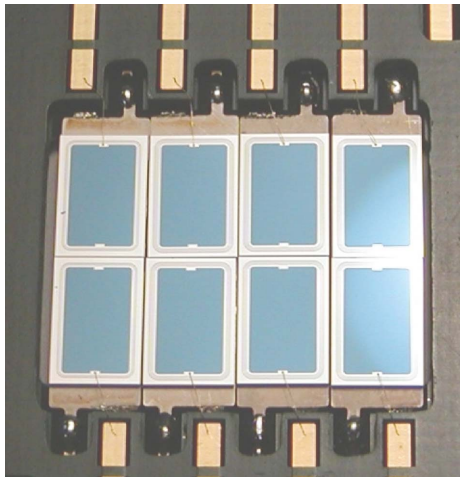

Figure 10
Photograph of an eight-channel assembled array from Hamamatsu. The active area of each element is 3 mm × 5 mm, with about 1 mm dead-space between devices. Note the mount is without backing, potentially allowing stacking of the arrays.

note that Hamamatsu has fabricated some special thin monolithic array devices using 50 μm-thick silicon (Kishimoto *et al.*, 2003). Stacking of this device is especially interesting for measuring nuclear inelastic scattering from isotopes with short lifetimes.

Hamamatsu also makes many different monolithic arrays based on their thinner epitaxic structures (active thickness <30 μm, *e.g.* S238X, S534X, S534X LC; see Table 2, and references therein). The dead-space between contacts on the front surface is typically 100 μm, with element sizes of 1 to 2 mm^2 and bond wires are used to make the contacts to the front of the device. Here we discuss one device (see Fig. 11) that was used for nuclear forward scattering (Baron *et al.*, 2001). This is a 16-element device, based on the S534X LC structure, with individual elements of 1 mm × 2.5 mm on a 1.1 mm pitch. Inclining the device at about 3° relative to the X-ray beam then gives a detector acceptance of about 0.8 mm × 2.5 mm and an effective increase of about ×20 in the active thickness perpendicular to the X-ray beam. This

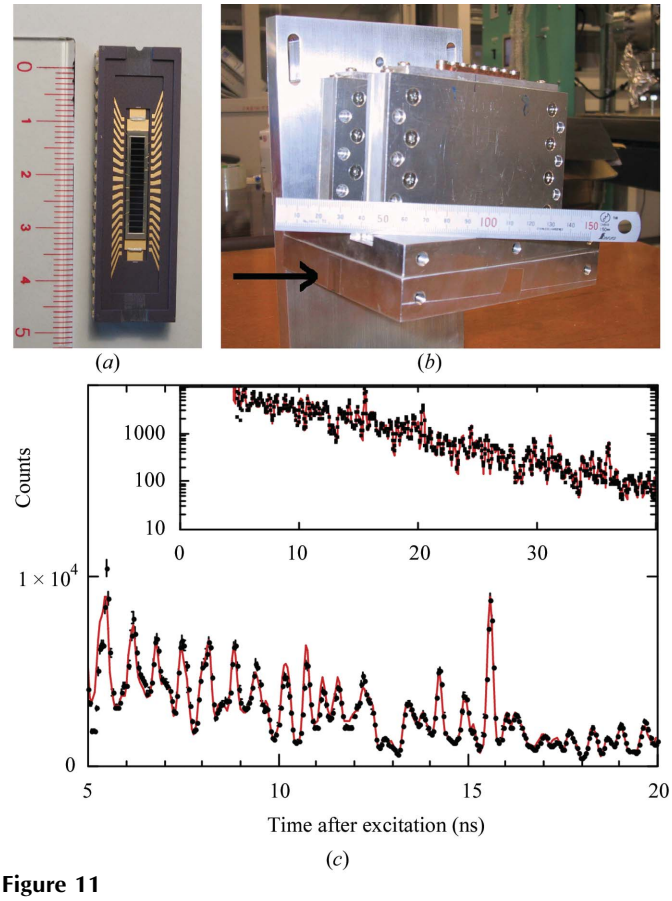

Figure 11
16-element array device from Hamamatsu. The device, in a standard 40 pin package, is shown in (*a*) while (*b*) shows the case including the dual eight-channel preamplifier modules above the main unit. The arrow shows the incident beam direction. The surface of the array is almost parallel (3° offset) to the X-ray beam direction. [Note that the device orientation in (*a*) is rotated by 90° relative to (*b*) for convenience in display.] In (*c*) the time response of ^{161}Dy in nuclear forward scattering on linear and log (inset) is shown. The solid line is a fit using the hyperfine parameters of the nucleus. Note the utility (necessity!) of the excellent time resolution in resolving the beat structure.

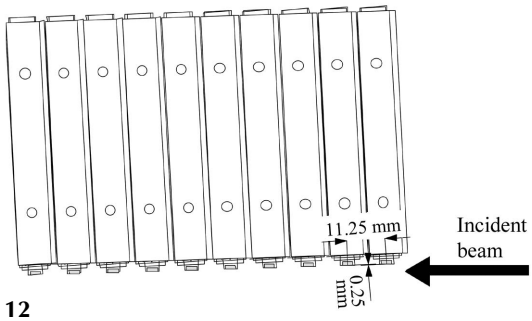

Figure 12
Schematic of the ten-channel modular array. Each module is 70 mm × 35 mm × 11 mm and includes an S5344 LC device (3 mm-diameter) and a pre-amplifier. Modules (and APDs) are individually replaceable. The beam is incident at about 3° relative to the APD surface. See text (§8) for more details.

then allows one to use the thin (∼20 µm active thickness) APD structure with correspondingly good time resolution (180 ps, when summed over all channels) for higher-energy X-rays. The device is shown in Figs. 11(*a*) and 11(*b*) while Fig. 11(*c*) shows the NFS spectrum measured using the ^{161}Dy resonance at 25.6 keV. Given the high-frequency response of this sample (up to 10 GHz) and the high energy of the resonance, the value of this sort of detector is clear. It is worth noting that special care was needed to assemble the two eight-channel pre-amplifier modules so that they did not oscillate.

An array of discrete elements, S5344 LC (3 mm-diameter), see Fig. 12, was also tested after successful work with the monolithic 16-channel array. This was partially motivated by lack of stability of the 16-element arrays,[4] and partially by the possibility of improving the detector, using larger elements that could be packaged and replaced individually. Also, though not the primary concern, the cost of the specialized monolithic array was greater than a set of individual standard devices. Ten modules, each with the APD and pre-amplifier, were assembled as shown in Fig. 12. Devices were selected so that operation with a common HV supply was possible. Tests with this device at 14.4 keV showed that it performed well. It is worth noting that the effective dead-area between devices (assuming perfect alignment) is 1 mm along the axis, owing to the silicon chip design with the 3 mm-diameter device on a 4 mm square chip, resulting in a loss of about 25% efficiency. Even so, the improvement in efficiency is quite significant (×20) using these at grazing incidence as compared with at normal incidence.

Many arrays have been fabricated based on beveled-edge devices (see Table 2). We have not tested them, and refer the interested reader to the listed references for details. It is worth noting, however, that to our knowledge these are the only cases of real square two-dimensional arrays with many elements, so, if such a device is of particular interest, these should be examined closely.

[4] Of three arrays tested, all showed wandering dark current after several days operation. In some cases this went away when the bias voltage was turned off for a while, but it also seemed to become progressively worse with time and in one case the device failed. Note that this might be related to contamination of the device surface, since the devices were delivered unsealed and handled in a laboratory environment, not a clean-room.

9. Conclusions

We have provided an overview of using APDs for fast detection of X-rays, emphasizing the relative merits of the various commercially available devices. In general, the 'fast-counter problem' for a single-element device seems largely solved by the sorts of devices discussed here, and the packages that have been made at synchrotron radiation facilities, with ∼ns time resolution basically for free. Things become slightly more complicated when high efficiency at high energy is required, or very good, *e.g.* 100 ps or less, time resolution is needed, or both. However, some of the array devices discussed in §8 may begin to provide solutions. Areas of immediate applicability of these devices include nuclear resonant scattering and also fast intensity correlation measurements, and applications can be expected to grow as more devices are optimized and packaged for synchrotron radiation work.

AQRB is grateful to Tetsuya Ishikawa for helping him continue work with APDs at SPring-8. Vital contributions were made in the development of the ESRF APD package system, by Pablo Fajardo-Sanz, Herve Gonzalez, Ricardo Hino of ESRF, and Francois Lissalde of Cyberstar SA. JM and J-MR also thank the numerous beamline staff at the ESRF who helped with practical tests of the system.

References

Baron, A. Q. R. (1994). *Nucl. Instrum. Methods*, A**352**, 665–667.
Baron, A. Q. R. (2000). *Hyperfine Interact.* **125**, 29–42.
Baron, A. Q. R. & Ruby, S. L. (1994). *Nucl. Instrum. Methods*, A**343**, 517–526.
Baron, A. Q. R., Rüffer, R. & Metge, J. (1997). *Nucl. Instrum. Methods*, A**400**, 124–132.
Baron, A. Q. R., Tanaka, Y. & Ishikawa, T. (2001). *SPring-8 Research Frontiers 2000/2001*, pp. 96–98. SPring-8, Hyogo, Japan.
Bateman, J. E. (2000). *J. Synchrotron Rad.* **7**, 307–312.
Brennan, S. & Cowan, P. L. (1992). *Rev. Sci. Instrum.* **63**, 850–853.
Carrier, C. & Lecomte, R. (1990). *IEEE Trans. Nucl. Sci.* **37**, 209–214.
Cromer, D. T. & Liberman, D. A. (1981). *Acta Cryst.* A**37**, 267–268.
Dieters, K., Ingram, Q., Musienko, Y., Nicol, S., Patel, P., Renker, D., Ruecroft, S., Rusack, R., Sakhelashvili, T., Swain, J. & Vikas, P. (2000). *Nucl. Instrum. Methods*, A**453**, 223–226.
Farrell, R., Shah, K., Vanderpuye, K., Grazioso, R., Meyers, R. & Entine, G. (2000). *Nucl. Instrum. Methods*, A**442**, 171–178.
Farrell, R., Vanderpuye, K., Cirignano, L., Squillante, M. R. & Entine, G. (1994). *Nucl. Instrum. Methods*, A**353**, 176–179.
Gerdau, E. & de Waard, H. (2000). Editors. *Hyperfine Interactions*, Vols. 123–125.
Gramsch, E., Szawlowski, M., Zhang, S. & Madden, M. (1994). *IEEE Trans. Nucl. Sci.* **41**, 762.
Gramsch, E., Zhang, S., Madden, M., Lindberg, M. & Szawlowski, M. (1993). *Proc. SPIE*, **2022**, 111–119.
Gullikson, E. M., Gramsch, E. & Szawlowski, M. (1995). *Appl. Opt.* **34**, 4662–4668.
Hara, K., Hata, K., Kikuchi, T., Kim, S., Kondo, K., Miyashita, S., Nakano, I., Okutomi, H., Sano, M., Seiya, Y., Takashima, S., Takikawa, K. & Tanaka, M. (1996). *Nucl. Instrum. Methods*, A**383**, 252–255.

Hauger, J. A., Choi, Y., Hirsch, A. S., Scharenberg, R. P., Stringfellow, B. C., Tincknell, M. L., Porile, N. T., Rai, G., Garbarino, J. & McIntyre, R. J. (1994). *Nucl. Instrum. Methods*, A**377**, 362–369.
Huth, G. C. (1968). *IEEE Trans. Nucl. Sci.* NS-**13**, 36–42.
Jacoboni, C., Canali, C., Ottaviani, G. & Quaranta, A. A. (1977). *Solid State Electron.* **20**, 77–89.
Kishimoto, S. (1991). *Nucl. Instrum. Methods*, A**309**, 603–605.
Kishimoto, S. (1992). *Rev. Sci. Instrum.* **63**, 824–827.
Kishimoto, S. (1994). *Nucl. Instrum. Methods*, A**351**, 554–558.
Kishimoto, S. (1995). *Rev. Sci. Instrum.* **66**, 2314–2316.
Kishimoto, S. (1997). *Nucl. Instrum. Methods*, A**397**, 343–353.
Kishimoto, S. (1998*a*). *J. Synchrotron Rad.* **5**, 275–279.
Kishimoto, S. (1998*b*). *J. Synchrotron Rad.* **5**, 883–885.
Kishimoto, S. (2004). *AIP Conf. Proc.* **705**, 881–884.
Kishimoto, S., Ishizawa, N. & Valasta, T. (1998). *Rev. Sci. Instrum.* **69**, 384–391.
Kishimoto, S., Yoda, Y., Seto, M., Kobayashi, Y., Kitao, S., Haruki, R. & Harami, T. (2003). *Nucl. Instrum. Methods*, A**513**, 193–196.
Knoll, G. F. (2000). *Radiation Detection and Measurement.* New York: Wiley.
Kuczewski, A. & Siddons, D. P. (2002). Unpublished.
Lecomte, R., Pepin, C., Rouleau, D., Dautet, H., McIntyre, R. J., McSween, D. & Webb, P. (1999). *Nucl. Instrum. Methods*, A**423**, 92–102.
Levin, C. S., Foudray, A. M. K., Olcott, P. D. & Habte, F. (2004). *IEEE Trans. Nucl. Sci.* **51**, 805–810.
Locker, R. J. & Huth, G. C. (1966). *Appl. Phys. Lett.* **9**, 227–230.
McIntyre, R. J. (1966). *IEEE Trans. Electron. Devices*, ED-**13**, 164.
McIntyre, R. J. (1972). *IEEE Trans. Electron Devices*, ED-**19**, 703–713.
McIntyre, R. J., Webb, P. P. & Dautet, H. (1996). *IEEE Trans. Nucl. Sci.* **43**, 1341–1346.
McMaster, W. H., Grande, N. K. D., Mallet, J. H. & Hubbell, J. H. (1969). *Compilation of X-ray Cross Sections.* Lawrence Radiation Laboratory, USA.
Moszynski, M., Kapusta, M., Balcerzyk, M., Szawlowski, M. & Wolski, D. (2000). *Nucl. Instrum. Methods*, A**442**, 230–237.
Moszynski, M., Szawlowski, M., Kapusta, M. & Balcerzyk, M. (2003). *Nucl. Instrum. Methods*, A**497**, 226–233.
Nonaka, N., Itoh, K., Nakamura, M., Niwa, K., Yamamoto, K. & Ishikawa, Y. (1996). *Nucl. Instrum. Methods*, A**383**, 81–88.
Rees, G. J. & David, J. P. R. (2003). *Proc. SPIE*, **4999**, 349–362.
Renker, D. (2002). *Nucl. Instrum. Methods*, A**486**, 164–169.
Shah, K. S., Farrell, R., Grazioso, R., Meyers, R. & Cirignano, L. (2001). *IEEE Trans. Nucl. Sci.* **48**, 2352–2356.
Shvyd'ko, Yu. V. (1999). Private communication.
Squillante, M. R., Reiff, G. & Entine, G. (1985). *IEEE Trans. Nucl. Sci.* NS-**32**, 563–566.
Sze, S. M. (1981). *Physics of Semiconductor Devices.* New York: Wiley.
Toellner, T. S., Sturhahn, W., Alp, E. E., Montano, P. A. & Ramanathan, M. (1994). *Nucl. Instrum. Methods*, A**350**, 595–600.
Trakalo, M., Webb, P. P., Poirrier, P. & McIntyre, R. J. (1987). *Appl. Opt.* **26**, 3594–3599.
Webb, P. P. & Dion, B. (1991). *Proc. SPIE*, **1563**, 236–243.
Webb, P. P. & Jones, A. R. (1974). *IEEE Trans. Nucl. Sci.* NS-**21**, 151–157.
Webb, P. P. & McIntyre, R. J. (1984). *IEEE Trans. Electron. Devices*, ED-**31**, 1206–1212.
Webb, P. P., McIntyre, R. J. & Conradi, J. (1974). *RCA Rev.* **35**, 234–278.
Yang, L., Dzhosyuk, S. N., Gabrielse, J. M., Huffman, P. R., Mattoni, C. E. H., Maxwell, S. E., McKinsey, D. N. & Doyle, J. M. (2003). *Nucl. Instrum. Methods*, A**508**, 388–393.